1-1-2022

ON STATISTICAL MODELS FOR SIGNAL DETECTION

Adedotun Michael Lawal

ON STATISTICAL MODELS FOR SIGNAL DETECTION

A Thesis

presented in partial fulfillment of requirements

for the degree of Masters of Science

in the Department of Physics

The University of Mississippi

by

ADEDOTUN M. LAWAL

May 2022

ABSTRACT

A thesis on developing statistical models that will aid in predicting signal detection at an infrasound sensor given a noise model for the sensor. The thesis aims first to provide a means to sample from a set of atmospheric profiles effectively using a statistical model, so we can have a smaller sample space to generate transmission loss values, saving time for running propagation models. And secondly, it aims to provide a formalism for a signal detection criterion using signal-to-noise ratio. The statistical model is developed using Empirical Orthogonal Function Analysis also known as Principal Component Analysis, and Inverse Transform Sampling. Further, we find the optimal sample size using a Cauchy criterion that indicates sampling optimally, which is the sample size the probability distribution converges. A joint probability density function is used to get the expectation value for the signal detection criterion and a measure of confidence in the expectation value. This thesis also presents probability distributions for transmission loss at different times and locations, majorly periods with a good ground duct and periods with a very bad ground duct. The probability distributions are produced using the Kernel Density Estimation approach. The probability distributions reveal the nature of the available ducts by showing high probability or low probability for a range of transmission loss values. Also, the atmospheric profiles used to generate the transmission loss for which we get probability distributions are those sampled from a large set of atmospheric profiles using the statistical model. This thesis has application in estimating what a source signal should be so detection can be made. It will be applied in the development of early warning systems for tornadoes.

DEDICATION

I dedicate this project to God Almighty, My Father, and My Lord Jesus Christ, who gave and is still giving himself for me. I also dedicate the project to my parents in Lord for being everything to me under the Lord Jesus Christ. Furthermore, I also dedicate this project to my family and brethren for their love towards me and being a major instrument of God in my life.

LIST OF ABBREVIATIONS AND SYMBOLS

g – Acceleration due to gravity

X – Random variable

c_{eff} – Effective sound speed

γ – Adiabatic index

R – Molar gas constant

τ_* – Optimal truncation location

(β) – Optimal hard threshold coefficient for unknown noise level

y_{med} – Median singular value

U – Uniform samples

h – Bandwidth

ACKNOWLEDGMENTS

All thanks to the Almighty God who has been gracious to me from the first day till now; all glory be to him. Thanks to The Lord Jesus Christ for his mercy throughout my academic duration.

All gratitude goes to my parents in the Lord. All of God's blessings go to my most wonderful family and brethren; Eternal Glorious Fountain Ministry worldwide.

Special thanks go to my family. I thank my Dad, Akinbohun Lawal, and Mum, Binlola Lawal, for their love towards me and for building a solid foundation for me. Also, I thank them for keeping a happy home; that was key in raising me and my younger ones, Adebowale Lawal and Ayomiposi Lawal. I love you, Adebowale Lawal and Ayomiposi Lawal; thank you for your place in my life and our parents' life

Gratitude goes to my wonderful advisor Dr. Roger Waxler for his ever present support towards this thesis. Also, a big thank you to Dr. Likun Zhang and Dr. Joel Mobley, who are members of the examining committee.

Also, it was a wonderful experience knowing Dr. Kevin Beach, the department's ex-graduate program coordinator. His constant support towards finishing my studies at the department is well appreciated. Also, thumbs up to Dr. Cecille Labuda, the current graduate program coordinator for the great work done so far and for picking up so fast in the position.

The infrasound group members have been fantastic. It was great working with Claus Hetzer; his prompt replies to technical issues are ones I really appreciate. Also thanks to April Kilpatrick for resolving all financial issues concerning the infrasound group.

Also, a big thank you to Garth Frazier for his technical support towards accomplishing this work.

Lastly, I say a huge thank you to all staff in the Department of Physics and Astronomy, the University of Mississippi, for their support towards the great work happening in the department.

TABLE OF CONTENTS

LIST OF FIGURES

CHAPTER 1

INTRODUCTION

Signal detection in infrasound involves detecting infrasonic signals at an infrasound sensor. Signal to noise ratio (SNR) is a concept used in engineering, finance, science, art. As the name implies, it is the ratio of signal-to-noise. The signal-and-noise could have several meanings depending on the field. For instance, in engineering and science, the signal and noise are the power of a signal and the power of noise, respectively. In user experience (UX), the signal is information on the user interface relevant to the user's current needs, and noise is otherwise. For our case in this thesis, signal refers to infrasound, and noise here is noise around an infrasound sensor. This thesis tries to provide a methodology for predicting if signal will be detected at a particular time by a sensor, if we have a noise model for such sensor.

In this thesis, we use a noise model developed by Max Willis [1]. The noise model is a probability distribution of rms pressure in dB. The noise here is a rms pressure as a function of frequency. The rms pressure was computed in the frequency band 0.4 Hz-4.0 Hz.

Signal would have undergone attenuation while propagating for it to be detected at some distance. This is where transmission loss, for which we developed probability distribution, comes up in this thesis. Transmission loss gives the factor by which the signal is attenuated in dB. Signal propagates through the atmosphere. The atmospheric state is a major determinant for infrasound

detection, the magnitude of transmission loss is dependent on it. Also, the atmospheric state, especially winds, which is a major factor in infrasound propagation, can be very dynamic; hence signal that would get to the sensor is also random – we can't always predict it.

The winds are one of the reasons why infrasonic signals can be detected at long distances from their sources. Also, the fact that the attenuation of infrasound is small allows them to be detected at long distances. Although for this work, we will be looking at infrasound propagation in regional distances, that is, distances less than 100km. In these distances, the winds alongside the temperature are primary propagation agents. The winds are not just a aid to the temperature in infrasound propagation but a major factor in infrasound propagation. They can generate infrasonic ducts that temperature cannot generate. This is illustrated in Figure 1.1.

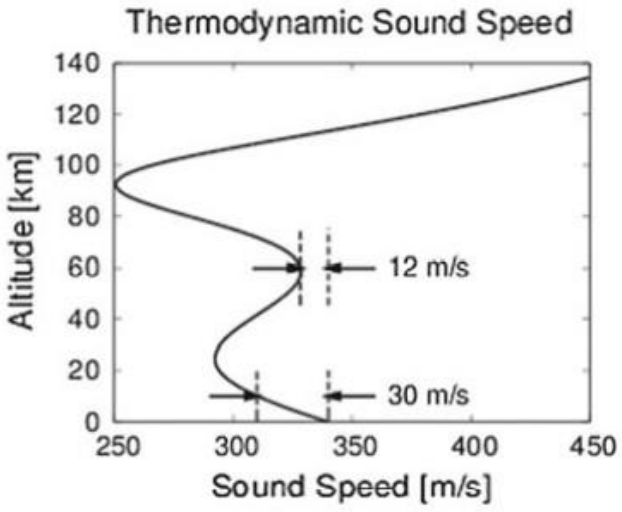

Figure 1.1: An atmosphere that cannot duct infrasound (R. Waxler, 2016, p. 3)

In Figure 1.1, we can see that the sound speed, a function of temperature, is lower at the stratopause than at the ground. This is not suitable for ducting infrasound, and signal will be trapped in the

atmosphere. This is usually the case at extreme latitudes, except at very cold times of the year. The wind hence become pivotal for infrasound propagation. For this work, we will deal with only the troposphere. From Figure 1.1, we can see that sound speed in the troposphere is lower than at the ground, which calls for wind for ducting. The wind that ducts in the troposphere is the jet stream; this is discussed in more detail in the next chapter.

This thesis builds models for the winds 12 years backward starting from 2021A.D. We look at the second week in January, April, August, and October. These months represent the four seasons of the year: winter, spring, summer, and fall. Also, we look at the hours, 05:00, 11:00, 17:00, 23:00 UTC for each day of the week considered.

CHAPTER 2

INFRASOUND PROPAGATION

Infrasound comes to play in several points of life, from natural occurrences - animal communication, thunderstorm, earthquake, etc. - to man-made activities like industrialization, wind turbines and even musical instruments (bass instruments), nuclear weapons, etc. Infrasound, often called low-frequency sound, is usually described as sound below the human hearing threshold, which is sound below 20 Hz, the lowest frequency that humans can typically hear. The range of human hearing extends up to about 20,000 Hz.

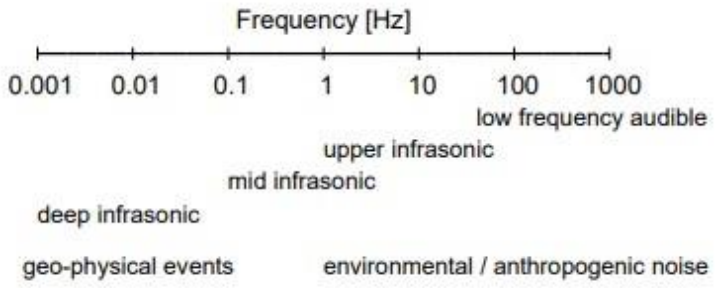

Figure 2.1: Decomposition of sound fields into frequency bands (R. Waxler, 2016, p. 1)

Figure 2.1 gives the characterization of sound that falls into the low-frequency audible range on a logarithmic scale into several frequency bands. There is a region in which sound propagates as acousto-buoyancy waves in which a distinction cannot be made between acoustic and buoyant

waves. They are labeled as deep infrasonic and can originate from meteors exploding in the middle atmosphere. This thesis will majorly deal with the mid-infrasonic band, which is about 0.1 Hz to a few Hz.

2.1 The Atmosphere: A Medium for Propagation

Propagation of infrasound occurs in the lower thermosphere downwards. Going downwards, we have the thermosphere, the mesopause (top of the mesosphere), the mesosphere, the stratopause (top of the stratosphere), the stratosphere, the tropopause (top of the troposphere), the troposphere. It is good to know that the atmosphere stratifies reasonably with temperature, as seen in Figure 2.2, which is why it serves as a medium of propagation. At the atmospheric boundary layer, say 1km, diurnal variation leads to complex behaviors in this region. However, above this region, things are quite stable as the temperature decreases with altitude till the tropopause, as seen in Figure 2.2. From the tropopause, the temperature starts to increase again till

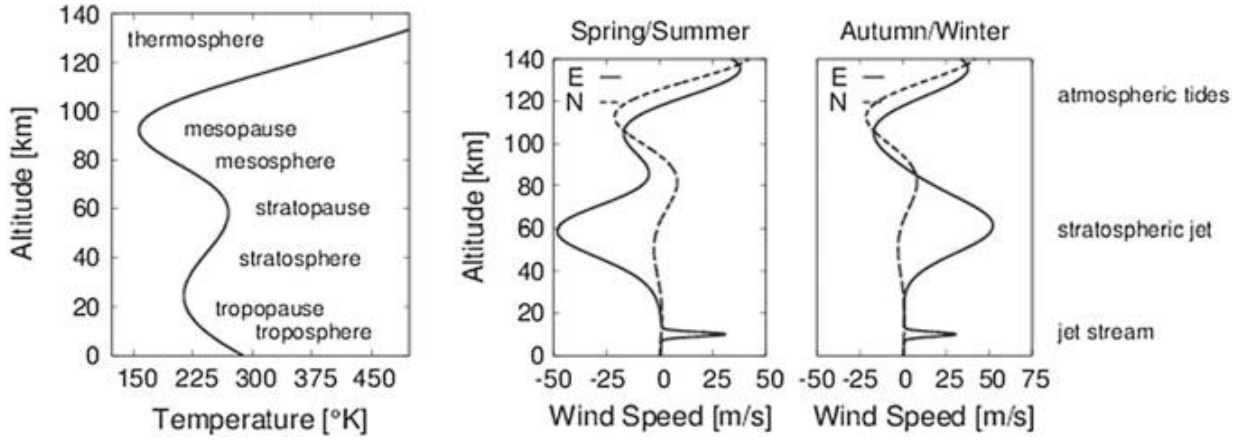

Figure 2.2: Variation of the atmosphere with altitude. The atmosphere is shown with temperature varying with altitude on the left, wind speed varying with altitude during Spring/Summer and Autumn/winter respectively in the center and right position (R. Waxler, 2016, p. 2)

the stratopause. It decreases till the mesopause and then increases through the thermosphere. For this thesis, we will only be concerned about the troposphere, as seen in Figure 2.3, and regional distances.

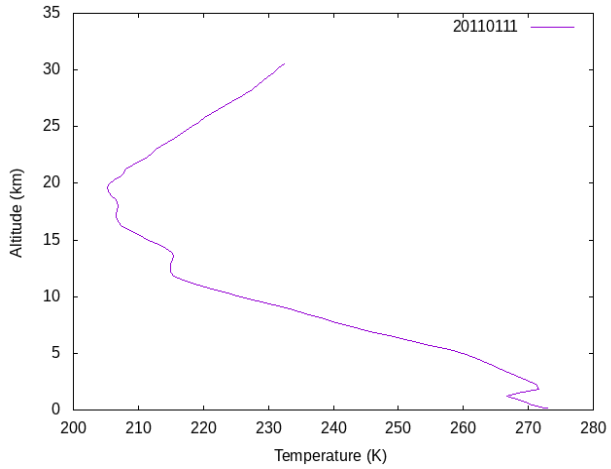

Figure 2.3: Temperature profile for the troposphere on January 11th, 2011.

2.2 The Atmospheric State

As mentioned in the first chapter, infrasound propagation is aided by temperature and wind in the atmosphere. Because the vertical changes in the atmosphere are on a greater scale than horizontal changes, the atmosphere is often taken to be vertically stratified. A hydrostatic equation of state can be represented for this vertical stratification under adiabatic conditions as

$$P_0(z) = P_0(0)e^{-\frac{g}{R}\int_0^z \frac{1}{T_0(z')}dz'} \tag{2.1}$$

using the ideal gas law $P_{0=}\rho_0 R T_0$

The mean temperature (T_0), entropy (S_0), pressure (P_0), density (ρ_0) depend on z as we expect vertical stratification to imply. Also, the mean entropy and density can be gotten from thermodynamic relations. The mean flow (wind) in the considered stratification, is give as

$$V_0 = \begin{pmatrix} V_{0,H} \\ 0 \end{pmatrix} = \begin{pmatrix} u \\ v \\ 0 \end{pmatrix} \tag{2.2}$$

where u and v are the standard atmospheric science notations for zonal and meridional wind speeds and are shown in Fig 2.4.

The winds are on a large scale and can be taken to have an influence that can make us treat them in a locally stratified approximation. Speaking of locally stratified approximation, small changes in the atmosphere horizontally can be accounted for by allowing the temperature and the wind to depend on location.

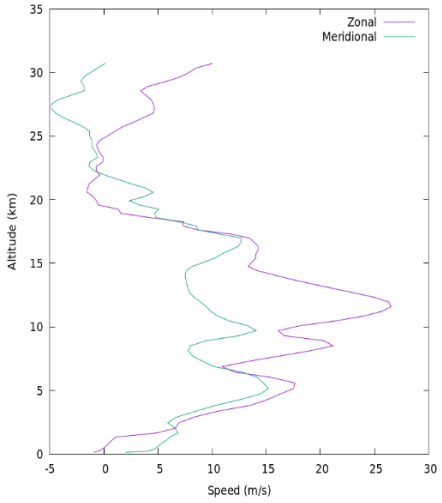

Figure 2.4: Wind speed profile showing the zonal and meridional wind speeds

2.3 Infrasonic Ducts

Sound is usually ducted by temperature and wind because sound is refracted by positive temperature gradients downwards and upwards by negative temperature gradients. This can be explained by Snell's law that signals refracts from regions of higher sound speed (v_1) that is regions with lower refractive index (n_1) to regions of lower sound speed (v_2) which is regions of higher refractive index (n_2). And since sound speed, c, for our purposes, has a relationship with temperature (T), it obeys the relation

$$c = \sqrt{\gamma RT} \tag{2.3}$$

where γ is the adiabatic index, R is the molar gas constant and T is the temperature.

This same manner applies for wind in which positive wind shear refracts downwards and negative upwards. As shown in Figure 1.1, the temperature at the ground is higher than that at the troposphere; hence according to Snell's law, sound will not be ducted (refracted) downwards - since as discussed above sound refracts downwards from regions of higher sound speed to regions of lower sound speed. Hence for sound to be ducted, the influence of wind is of great advantage. This is where the tropospheric jet comes in to help with ducting. Since for there to be downward refraction, there is a need for regions above with higher sound speed than the ones below according to snell's law. It is also good to know that sound is ducted downwind and refracted away from the earth upwind.

2.3.1 Effective Sound Speed

For our purposes in this thesis, we will not work directly with the atmospheric specifications given above, zonal and meridional wind speed, but with effective sound speed (c_{eff}).

The effective sound speed is the sum of the sound speed (c) and the horizontal component of wind speed (u_0) in the direction of propagation, and is given by

$$c_{eff}(z) = c(z) + u_0(z) \tag{2.4}$$

It is good to note that the effective sound speed is only valid for low grazing angles and small Mach numbers (M << 1), as it overestimates the effect of horizontal wind on sound propagation, leading to errors in traveltime and propagation path, trace velocity, and absorption [3]. The effective sound speed is the sound speed at the duct. It reflects clearly what regions in the atmosphere will produce a duct given a propagation azimuth. Also, the effective sound speed concept is used to reduce the complexity of the governing equations for infrasound propagation models [4].

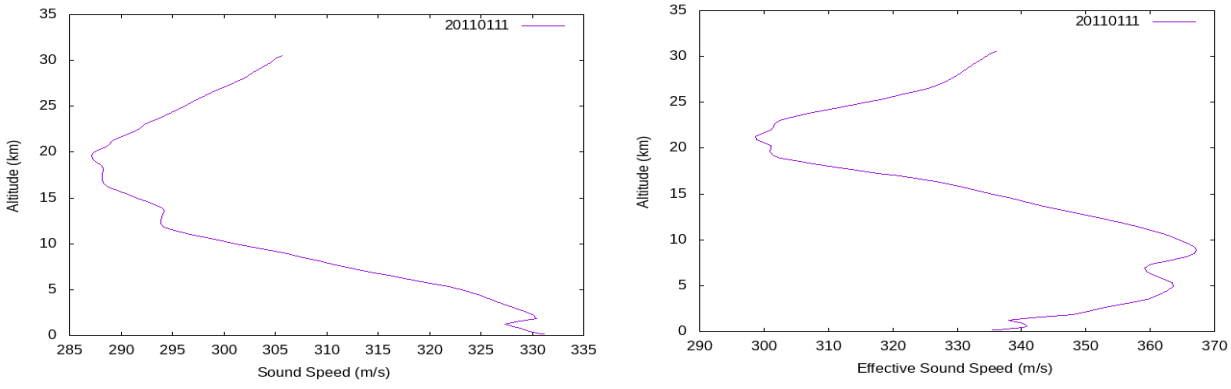

(i) (ii)

Figure 2.5: Sound speed and effective sound speed profiles. (i) shows a sound speed profile on January 11th, 2011 and (ii) shows an effective sound speed profile along the 90º azimuth (north) on January 11th, 2011.

2.3.2 The Tropospheric Duct

The jet stream causes the tropospheric duct in the troposphere. It is located about 10 km from the Earth's surface. Signal returns due to tropospheric ducting can be measured about 100 km from the source.

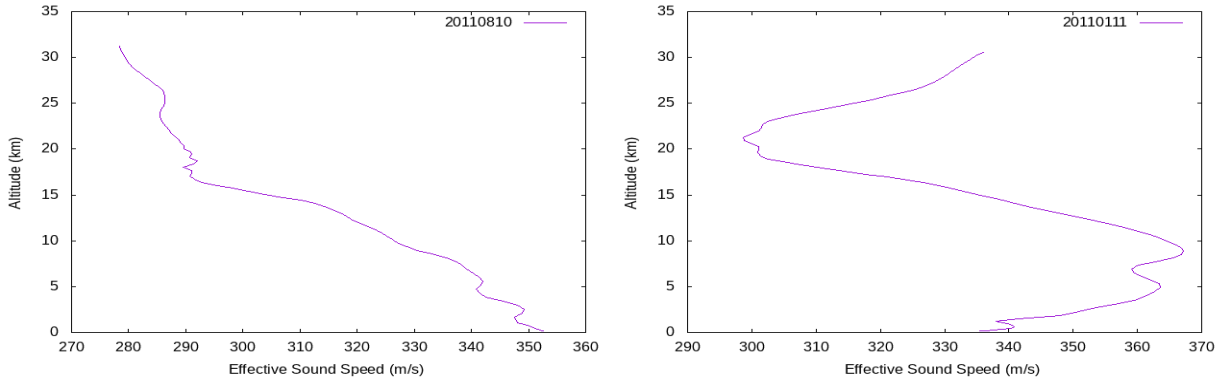

(i) (ii)

Figure 2.6: Effective sound speed profiles. (i) an effective sound speed profile that will give a good ground duct and (ii) an effective sound speed profile that will give a bad ground duct in the troposphere.

The tropospheric duct varies in magnitude and direction seasonally. During the winter, spring and fall, there is usually a large eastward flow, and during the summer, a small eastward and westward flow occur. Figure 2.6 (i) and Figure 2.7 (i) show effective sound speed profile and 2D transmission loss plot for the summer period in which the tropospheric jet is not as strong as in other seasons. This is expected to give a bad ground duct, evident from Figure 2.7 (i).

The atmospheric profiles used in this thesis are gotten from the Weather Research and Forecasting (WRF) model [5]. Other sources of atmospheric profiles are the Ground-to-Space (G2S) and European Centre for Medium-Range Weather Forecast (ECMWF).

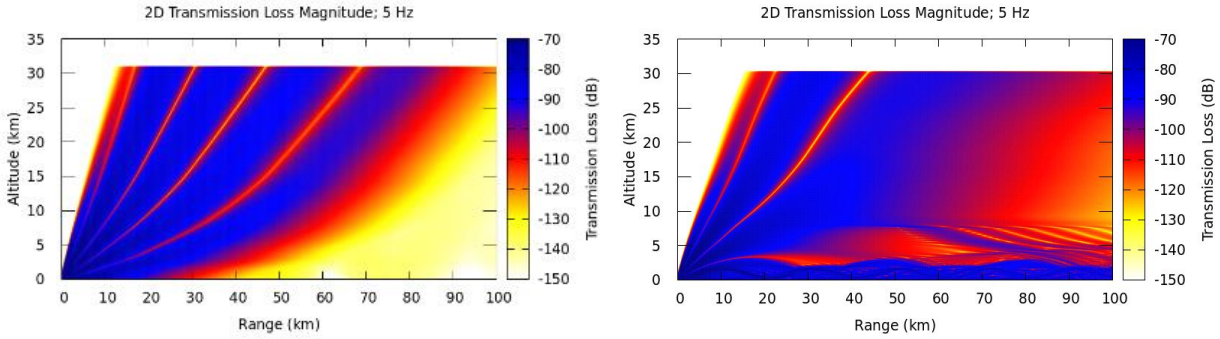

(i) (ii)

Figure 2.7: 2D Transmission loss plots. (i) shows the corresponding 2D Transmission loss plot for the effective sound speed profiles in Figure 2.6 (i), and (ii) shows the corresponding 2D Transmission loss plot for the effective sound speed profiles in Figure 2.6 (ii)

2.4 Propagation Model

This thesis uses a propagation model to estimate the transmission loss of infrasound along propagation paths in the atmosphere. The propagation model used in this thesis is the NCPA (National Centre for Physical Acoustics) ePape (Effective Sound Speed Pade Parabolic Equation Code)[6]. It is a parabolic equation model (P.E. model). The influence of wind is approximated using the effective sound speed approximation. EPape is fullwave and non-linear. EPape supports the range-dependent and stratified atmosphere. For this thesis, we use a stratified atmosphere. The functions of the differential operators that arise are approximated using a Padé expansion whose order can be specified. The Padé expansion is numerically efficient when dealing with high elevation angles, although the effective sound speed approximation limits the azimuth used (shallow angle approximation). EPape outputs transfer functions for propagation from a unit point source at a reference distance of 1 km. The transfer functions have an imaginary and real part, and the magnitude of the transfer functions gives the signal attenuation. The transmission is the signal attenuation in dB relative to 1.

CHAPTER 3

EMPIRICAL ORTHOGONAL FUNCTION ANALYSIS

3.1 Empirical Orthogonal Function Analysis

Empirical Orthogonal Function (EOF) analysis is a process of decomposing information (data) in terms of basis functions called Empirical Orthogonal Functions (EOF). This method is similar to eigenfunction expansion, and the basis functions are derived from the data. The EOF analysis is used for two reasons; one is to produce a one-dimensional distribution of the coefficients of the EOFs from which we can sample, and two, to have a smaller sample space to sample from by truncating optimally. In summary, the EOF analysis is used in conjunction with inverse transform sampling to sample efficiently.

The EOF analysis' underlying method is the singular value decomposition (SVD). The SVD is one of the most used linear algebra methods for processing data. The SVD decomposes data into a left orthogonal matrix, a matrix of singular values, and a right orthogonal matrix. It is good to see the SVD as a linear algebra generalization of the Fourier series. Instead of having the orthogonal functions as the right and left singular vectors, we have them as sine and cosine functions. The sampled data from the EOF analysis can represent the real data. This is because the first few EOFs, which we will see later as the first few right singular vectors, give the most significant part of the information (data). And this is because the singular values are arranged so that the first one is the most important. The second gives the next most important and so on. Hence

choosing only the first few singular values which correspond to the first few EOFs gives us a good representation of the real data. The other singular values and EOFs can be ignored as they contain very little information about the real data.

Mathematically, we represent the SVD of a matrix X as

$$X = U\Sigma V^{*} \tag{3.1}$$

U is a matrix of the left orthogonal vectors, Σ is a diagonal matrix of singular values and V* is a matrix of the right orthogonal vectors. U and V are unitary matrices. In computing the SVD of a matrix, we always get the full SVD, as shown in Figure 3.1.

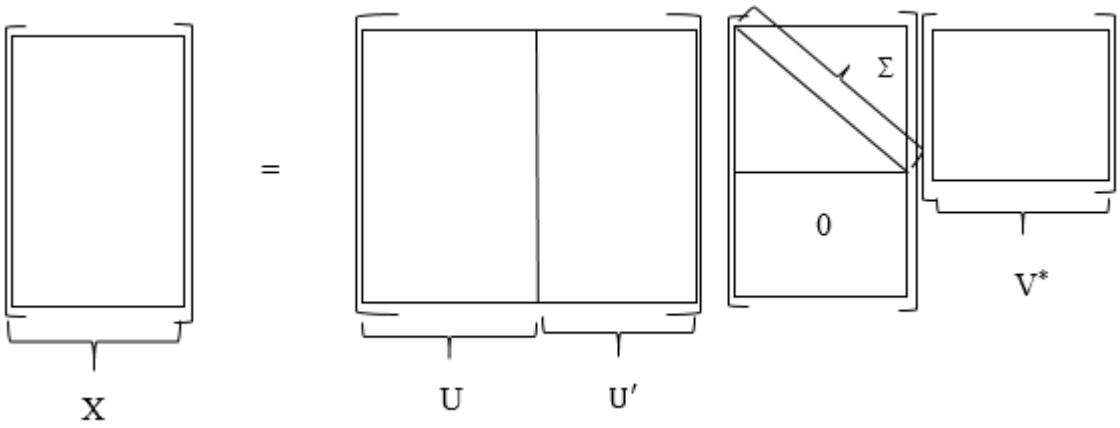

Figure 3.1: The Full SVD

However, what most computational algorithms compute is the Economy SVD, seen in Figure 3.2. This is obviously because in the reconstruction of matrix X, which is done by an outer product, the zeros in the singular value matrix, reduce matrix U.

Furthermore, because the first few singular values correspond to most of the variance, we usually truncate the Economy SVD to singular values and orthogonal matrices corresponding to

the first few singular values. This gives us a truncated SVD, as seen in Figure 3.3. The truncated SVD provides a smaller number of coefficients of EOFs to sample from.

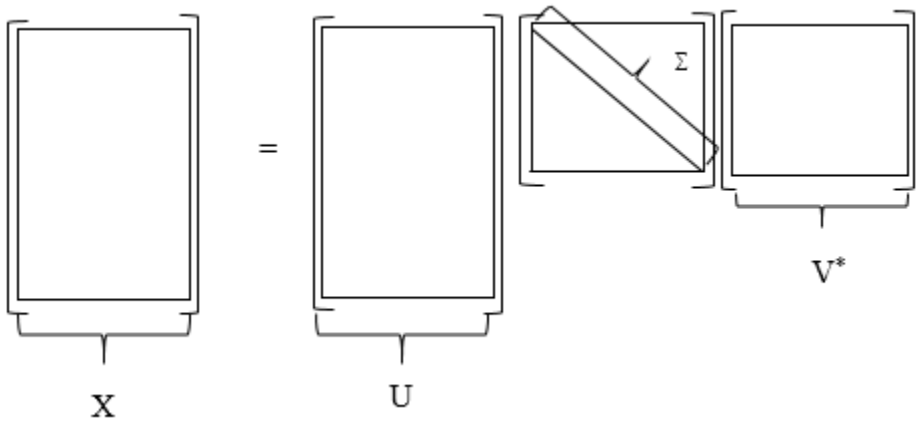

Figure 3.2: The Economy SVD.

The optimal location to truncate is given by Donoho *et al* (2013) as

$$\boldsymbol{\tau}_* = \boldsymbol{\omega}(\boldsymbol{\beta}).\, \mathbf{y_{med}} \tag{3.2}$$

Where $\boldsymbol{\tau}_*$ is the optimal location, **(β)** is the optimal hard threshold coefficient for unknown noise level and $\boldsymbol{y_{med}}$ is the median singular value, where

$$\boldsymbol{\omega}(\beta) \approx 0.56\beta^3 - 0.95\beta^2 + 1.82\beta + 1.43. \tag{3.3}$$

β is m/n for a m by n matrix.

It is good to note that the EOFs are the rows of the right orthogonal matrix. The truncated SVD can be seen below.

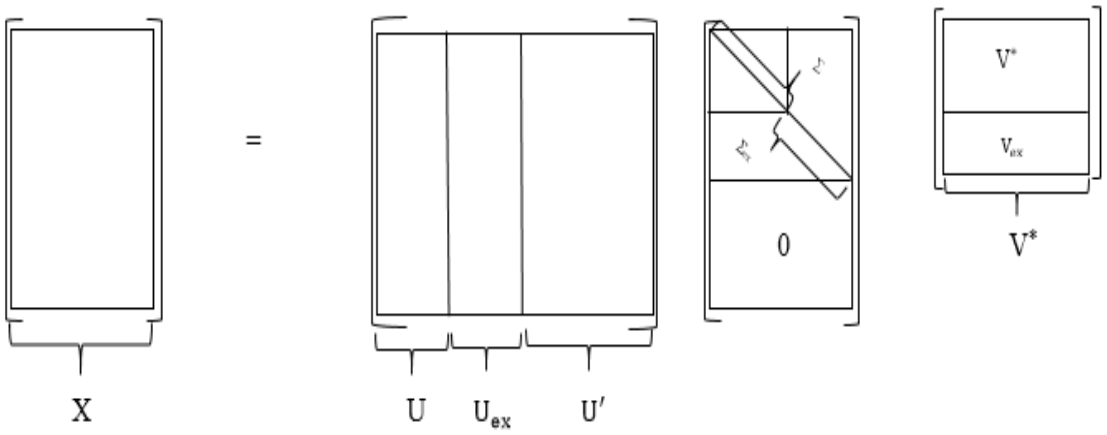

Figure 3.3: The Truncated SVD

In the truncated SVD, which we get from the economy and full SVD, the left orthogonal matrix contains the r-leading columns of U. The singular matrix contains the leading r by r sub-block of Σ, and the right orthogonal matrix contains the r-leading columns of V. $U_{ex}, \Sigma_{ex}, V_{ex}$ correspond to the left orthogonal matrix, matrix of singular values, and right orthogonal matrix, respectively, considered less important, as they cover little variance of the data. Hence the matrix reconstructed from truncated SVD can effectively represent the original matrix X; this is shown in Figure 3.4 and Figure 3.5. These figures show that there is almost no difference between the original data and those reconstructed with the first r left singular vectors, or EOFs, as we will prove soon.

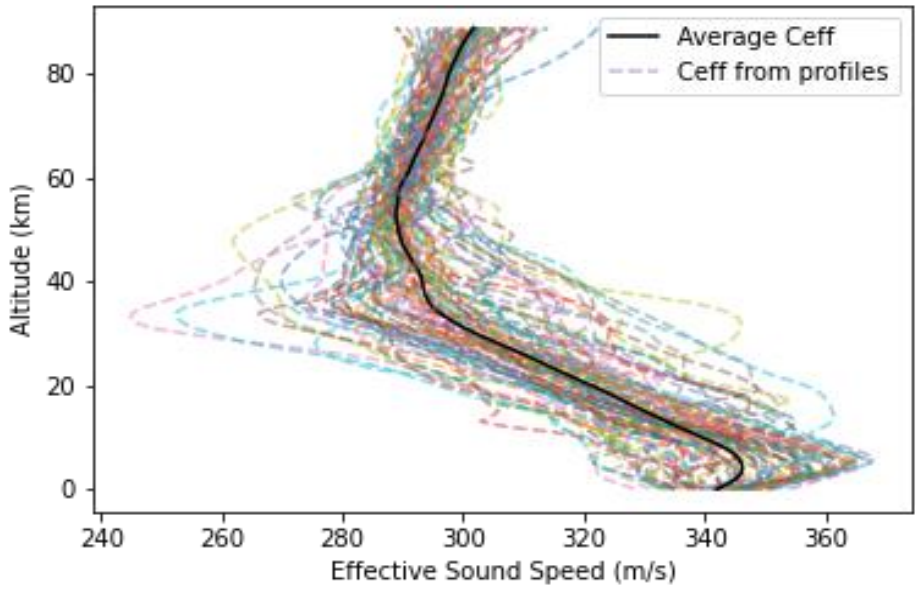

Figure 3.4: Effective sound speeds and average effective sound speed vector profiles.

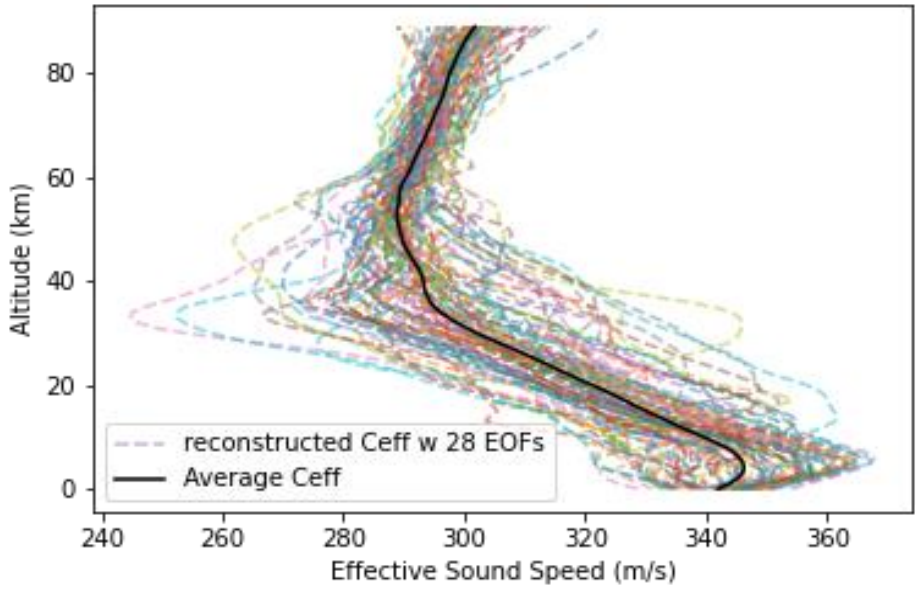

Figure 3.5: Reconstructed effective sound speeds and average effective sound speed vector profiles.

In this thesis, there is a need to understand how the SVD relates to eigendecomposition. This is because we represent the effective sound speed as a vector, and the EOFs serve as its basis vectors. The basis vector coefficients are the product of the right orthogonal vectors and the singular values. The way we use the SVD is that a vector is anything that transforms. A vector, in our case, the effective sound speed, can be written as a linear combination of basis vectors. We can prove that these basis vectors are the V*.

Let A be X*X so that we can solve an eigenvalue problem. In solving an eigenvalue problem, we have that

$$AF = FL \tag{3.4}$$

Where columns of F are the eigenvectors, F is unitary, and the leading diagonal of L are the eigenvalues.

Also recall that SVD of X gives $U\Sigma V^*$. And we can have

$$A = FLF^* \tag{3.5}$$

Since F is unitary and $F^{-1} = F^*$

From $A = X^*X$, expressing X in a singular value decomposed form, we can have

$$A = (U\Sigma V^*)^*(U\Sigma V^*) \tag{3.6}$$

Hence we can have

$$A = V\Sigma^* U^* U\Sigma V^* \tag{3.7}$$

We know that for unitary matrices, which U is, $U^*U = 1$

$$A = V\Sigma^{*}\Sigma V^{*} \tag{3.8}$$

comparing the (3.8) and (3.5)

we see that $\Sigma^{*}\Sigma$ = L and V = F

This proves that the right orthogonal vectors, the EOFs, can serve as a basis of a matrix we construct for our effective sound speed. If we have a matrix of our effective sound speed and subtract an average effective sound speed vector from it and call it X, the coefficients of EOFs of X are statistically independent. We can expand X in terms of its EOFs to get

$$X = \sum_{i=1}^{r} C_i V_i^{*} \tag{3.9}$$

It is good to note that $C_i = U_i\Sigma_i$, the product of a left singular vector, and its corresponding singular value, is gotten from the SVD of X. Also, we use the truncated SVD, that is, the SVD with r singular values, r EOFs, and r right singular vectors.

Let the difference between an effective sound speed vector and the average effective sound speed vector be ΔC_{eff}^{j}, delta effective sound speed vector, and be given as

$$\Delta C_{eff}^{j} = C_{eff}^{j} - < C_{eff} > \tag{3.10}$$

$< C_{eff} >$ is just

$$< C_{eff} > = \frac{1}{n}\sum_{j=1}^{n} C_{eff}^{j} \tag{3.11}$$

ΔC_{eff}^{j} can be expanded in terms of its EOFs to give us

$$\Delta C_{eff}^{j} = \sum_{i=1}^{r} C_i^{j} E_i \tag{3.12}$$

and C_i^j can be written as

$$C_i^j = E_i . \Delta C_{eff}^j \tag{3.13}$$

also, the average coefficient of an EOF is given by

$$< C_i > = \frac{1}{n} \sum_{j=1}^{n} C_i^j \tag{3.14}$$

from (3.14) we have

$$< C_i > = \frac{1}{n} \sum_{j=1}^{n} (E_i . \Delta C_{eff}^j) \tag{3.15}$$

Also we can write the average delta effective sound speed vector

$$<\Delta C_{eff} > = \frac{1}{n} \sum_{j=1}^{n} \Delta C_{eff}^j \tag{3.16}$$

From (3.15) and (3.16) we have

$$< C_i > = E_i .<\Delta C_{eff} >. \tag{3.17}$$

Now to prove that the coefficients of the EOFs are statistically independent, the following must show that

$$\langle (C_i - < C_i >)(C_{i'} - < C_{i'} >) \rangle = 0 \tag{3.18}$$

That is the variance of the two coefficients of EOFs must give 0

$$\frac{1}{n} \sum_{j=1}^{n} (C_i^j - < C_i >)(C_{i'}^j - < C_{i'} >) = 0 \tag{3.19}$$

However, $< C_i >$ can be proved to be 0

From (3.17) we have that

$$< C_i > = E_i.<\Delta C_{eff} >$$

Substituting (3.10) in (3.17) we have

$$< C_i > = E_i.\langle \left(C_{eff}^j - < C_{eff} >\right) \rangle \quad (3.20)$$

this can be written as

$$< C_i > = E_i.\left(\frac{1}{n}\sum_{j=1}^{n}\left(C_{eff}^j - < C_{eff} >\right)\right) \quad (3.21)$$

Further, we can write (3.21) as

$$< C_i > = E_i.\left(\frac{1}{n}\sum_{j=1}^{n} C_{eff}^j - \frac{1}{n}\sum_{j=1}^{n} < \Delta C_{eff} >\right) \quad (3.22)$$

However, from (3.16) we have that

$$< C_i > = E_i.\left(< \Delta C_{eff} > - \frac{1}{n}\sum_{j=1}^{n} < \Delta C_{eff} >\right) \quad (3.23)$$

also, because $< \Delta C_{eff} >$ is the average effective sound speed vector we have,

$$\frac{1}{n}\sum_{j=1}^{n} < \Delta C_{eff} > = < \Delta C_{eff} >$$

that is you cannot sum over j, thus (3.23) will give 0.

Now (3.19) can be written as

$$\frac{1}{n}\sum_{j=1}^{n} (C_i^j)(C_{i'}^j) = 0 \quad (3.24)$$

Using (3.13) we have that

$$\frac{1}{n}\sum_{j=1}^{n}\ (E_i.\Delta C_{eff}^{j})(E_{i'}.\Delta C_{eff}^{j}) \tag{3.25}$$

It can be proved that $\sum_{j=1}^{n}\ (E_i.\Delta C_{eff}^{j})(E_{i'}.\Delta C_{eff}^{j}) = E_i.(XX^TE_{i'})$ (3.26)

To prove this recall that X is a matrix of the delta effective sound speed vectors.

$$\begin{pmatrix} \Delta C_{eff}^{1}(z_1) & \cdots & \Delta C_{eff}^{n}(z_1) \\ \vdots & \ddots & \vdots \\ \Delta C_{eff}^{1}(z_m) & \cdots & \Delta C_{eff}^{n}(z_m) \end{pmatrix} \tag{3.27}$$

and X^T can be written as

$$\begin{pmatrix} \Delta C_{eff}^{1}(z_1) & \cdots & \Delta C_{eff}^{1}(z_m) \\ \vdots & \ddots & \vdots \\ \Delta C_{eff}^{n}(z_1) & \cdots & \Delta C_{eff}^{n}(z_m) \end{pmatrix} \tag{3.28}$$

In proving (3.26), we can write $X^TE_{i'}$ as

$$\begin{pmatrix} \Delta C_{eff}^{1}(z_1) & \cdots & \Delta C_{eff}^{1}(z_m) \\ \vdots & \ddots & \vdots \\ \Delta C_{eff}^{n}(z_1) & \cdots & \Delta C_{eff}^{n}(z_m) \end{pmatrix} \begin{pmatrix} E_{i'}(z_1) \\ \vdots \\ E_{i'}(z_m) \end{pmatrix} \tag{3.29}$$

and it gives us

$$\begin{pmatrix} \Delta C_{eff}^{1}.E_{i'} \\ \vdots \\ \Delta C_{eff}^{n}.E_{i'} \end{pmatrix} \tag{3.30}$$

further in proving 3.26, using (3.27) and (3.30)

$$XX^TE_{i'} = \begin{pmatrix} \Delta C_{eff}^{1}(z_1) & \cdots & \Delta C_{eff}^{n}(z_1) \\ \vdots & \ddots & \vdots \\ \Delta C_{eff}^{1}(z_m) & \cdots & \Delta C_{eff}^{n}(z_m) \end{pmatrix} \begin{pmatrix} \Delta C_{eff}^{1}.E_{i'} \\ \vdots \\ \Delta C_{eff}^{n}.E_{i'} \end{pmatrix}$$

and multiplying the matrices, we have

$$XX^{T}E_{i'} = \begin{pmatrix} \Delta C^{1}_{eff}(z_1)\Delta C^{1}_{eff}.\,E_{i'} & + & \cdots & \Delta C^{n}_{eff}(z_1)\Delta C^{n}_{eff}.\,E_{i'} \\ \vdots & & \ddots & \vdots \\ \Delta C^{1}_{eff}(z_m)\Delta C^{1}_{eff}.\,E_{i'} & + & \cdots & \Delta C^{n}_{eff}(z_m)\Delta C^{n}_{eff}.\,E_{i'} \end{pmatrix} \tag{3.31}$$

(3.31) can be written as

$$\sum_{j=1}^{n} \begin{pmatrix} \Delta C^{j}_{eff}(z_1)\Delta C^{j}_{eff}.\,E_{i'} \\ \vdots \\ \Delta C^{j}_{eff}(z_m)\Delta C^{j}_{eff}.\,E_{i'} \end{pmatrix} \tag{3.32}$$

finally, $E_i.(XX^{T}E_{i'})$ will give us

$$E_i.\sum_{j=1}^{n} \begin{pmatrix} \Delta C^{j}_{eff}(z_1)\Delta C^{j}_{eff}.\,E_{i'} \\ \vdots \\ \Delta C^{j}_{eff}(z_m)\Delta C^{j}_{eff}.\,E_{i'} \end{pmatrix} \tag{3.33}$$

(3.33) can be written as

$$\sum_{j=1}^{n} E_i.\,\Delta C^{j}_{eff}\Delta C^{j}_{eff}.\,E_{i'} \tag{3.34}$$

Since ΔC^{j}_{eff} and E_i are column vectors, we can apply the commutative property of dot product to give us

$$\sum_{j=1}^{n} E_i.\,\Delta C^{j}_{eff}E_{i'}.\,\Delta C^{j}_{eff} \tag{3.35}$$

Thus we see that (3.26) is proved.

Now (3.25) can be written as

$$\frac{1}{n}E_i.(XX^{T}E_{i'}) \tag{3.36}$$

However, since XX^T is a square matrix and $E_{i'}$ is a basis vector, (3.36) can be written in terms of eigenvalues and eigenvectors to give

$$\frac{1}{n} E_i . (\lambda E_{i'}) \tag{3.37}$$

λ is an eigenvalue.

We can rewrite (3.37) as

$$\frac{\lambda}{n} E_i . E_{i'} \tag{3.38}$$

and further have it as

$$\delta_{ii'} \frac{\lambda}{n} \tag{3.39}$$

Also,

$$\lambda = S_{i'}^2 \tag{3.40}$$

where $S_{i'}$ is the i'th singular value.

Thus (3.39) gives us

$$\delta_{ii'} \frac{S_{i'}^2}{n} \tag{3.41}$$

For $E_i \neq E_{i'}$ (3.41) gives 0.

Now (3.18) is proved; the coefficients of EOFs are statistically independent.

This allows us to use inverse transform sampling and reconstruct by taking an inner product with the EOFs, to get the desired number of samples we want, as we will see in the next chapter.

3.2 Kernel Density Estimate

The kernel density estimate (KDE) is a density estimator for an unknown probability distribution. The KDE is like the histogram but with a smooth function. The smooth function is called the kernel, hence the name kernel density estimate. We have different kernels; some are gaussian, epanechnikov, exponential, cosine etc.

In this thesis, we will be using the gaussian kernel. This is because most real-life random processes have a distribution that is close to the normal distribution. The KDE works by using a gaussian distribution function centralized at the data point. The overlapping estimates from the gaussian distributions centralized at data points are then summed at all overlapping points to give the main KDE curve.

Like a histogram, binning is a major consideration for KDE as small bins give noisy data and too large bins obscure information. Hence choosing a good bin size is pivotal for the kernel density estimate. A rule for binning used in this project is from the Improved Sheather-Jones algorithm. It is good for multimodal data.

The KDE is a non-parametric method of assigning a probability distribution curve to data whose probability distribution is unknown. The probability function is the sum of the kernel functions at each data point. Mathematically, we have it as

$$\frac{1}{nh}\sum_{i=1}^{n} K\left(\frac{x-x_i}{h}\right) \tag{3.42}$$

Where K is the kernel, x_i are the locations of the kernels and, x is a sample from data, h is the bandwidth, n is the number of data points

CHAPTER 4

SAMPLING THEORY

Sampling is simply the process of taking a subset from a population. As mentioned earlier in this thesis, we sample using inverse transform sampling and EOF analysis. The motivation for using the EOF analysis is based on its underlying algorithm, the SVD. Furthermore, the motivation for considering a method that uses the SVD is because the SVD generalizes an eigendecomposition for non-square matrices. And the motivation for eigendecomposition is because we know that the coefficients of the EOFs (basis vectors) are statistically independent.

4.1 Inverse Transform Sampling

Inverse transform sampling is a method of sampling in statistics in which samples are generated from a given probability distribution given that we have its cumulative distribution function (CDF). This works by using uniform samples, samples from a uniform distribution, between 0 and 1, which are used as independent variables of an inverse cumulative distribution function. The uniform samples, in this case, serve as probabilities the associated probability distribution.

This method is also used as a means of sampling from an arbitrary probability distribution, given the CDF is known, and it can be inverted to get an inverse function. It is good to know that this works for a discrete and continuous distribution.

Mathematically, given that the cumulative distribution function is

$$G(x) = P(X \leq x) \tag{4.1}$$

This gives the probability of getting a random variable x or less.

We can invert it to get an inverse function

$$G^{-1} \tag{4.2}$$

Uniform samples (U) can be used in the inverse function as independent variables to give us samples with the probability distribution of the CDF. Mathematically, we have

$$G^{-1}(U) = X \tag{4.3}$$

The samples we want are X.

The inverse transform sampling method is used to get the desired number of samples. It works because the coefficients of the EOFs are statistically independent; hence we can have a probability distribution for each set of coefficients, and from it, we get the cumulative distribution function. We invert the cumulative distribution function to get the inverse cumulative distribution, and we sample using a random number generator. The sampled coefficients are reconstructed with the EOFs to get a sample effective sound speed. The sample effective sound speed we got is passed into ePape, to simulate transmission loss values. We construct a KDE for these transmission loss values, repeat the process, and accumulate the transmission loss values with the first one. We get a KDE for it, which would differ from the KDE of the first transmission loss values only. We repeat this process until the KDE converges; it stops changing. This convergence criterion is the convergence criteria of a sequence. In this case, we use the Cauchy criterion, and the sequence is

the sequence of KDE obtained from the sampling method. As we keep increasing the number of samples, the KDE should eventually converge to the correct KDE.

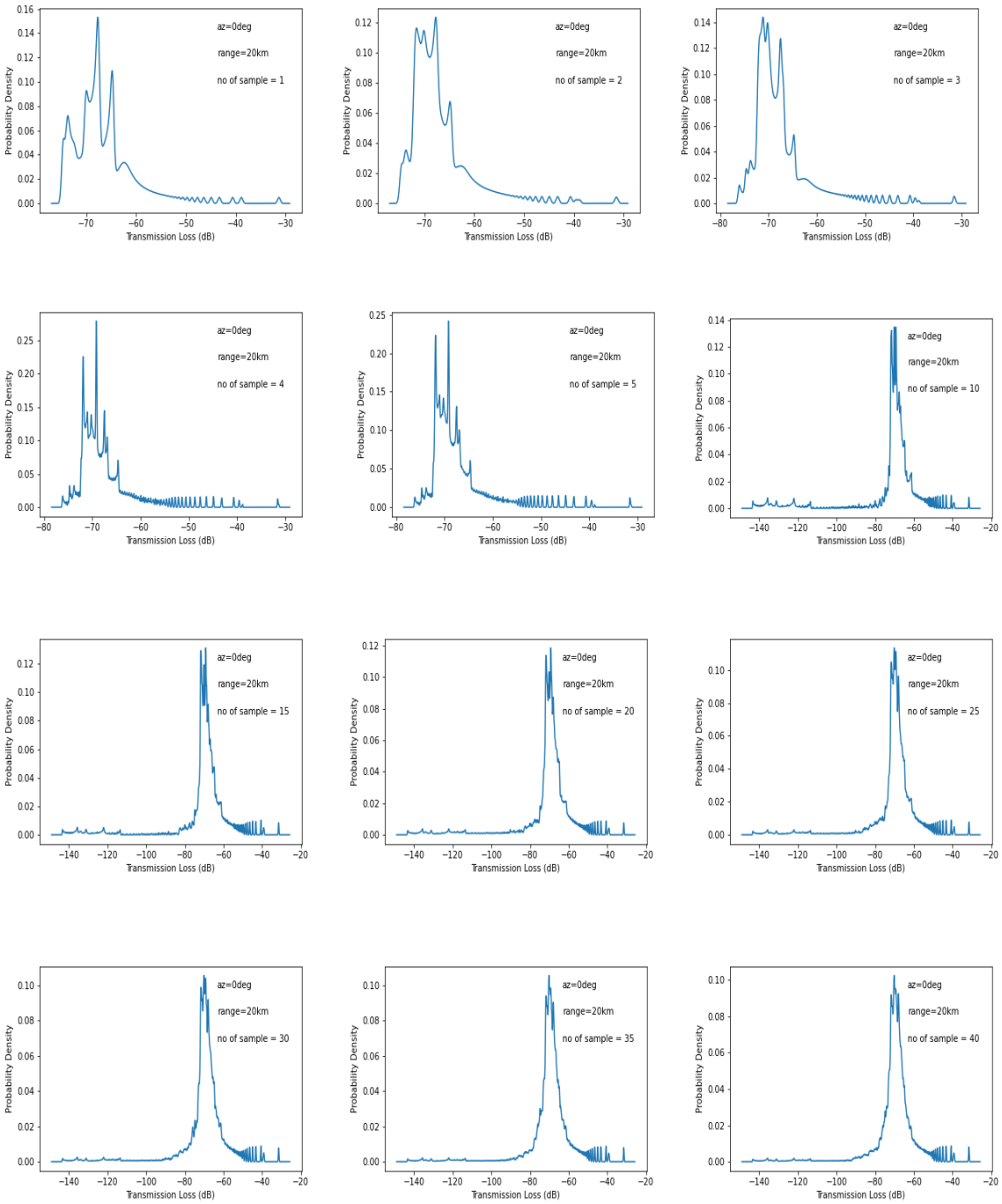

Figure 4.1: Transmission loss KDE convergence.

In mathematics, the Cauchy criterion is satisfied when, for all a, there is a fixed number N such that $|S_j - S_i| < \epsilon$ for all i, j > N. In our case, S_j and S_i are the accumulated transmission values we get KDEs for. This convergence criterion helps us get the optimal sample size.

CHAPTER 5

RESULTS

This session presents the KDE plots for transmission loss at particular hours -5th, 11th, 17th, and 23rd - on all days in the second week of January, April, August, and October. Atmospheric profiles for 12 years (2010 – 2021 A.D.) were used. We simulated transmission loss for ranges 20 km, 40 km, 60 km, and 80 km. This result reveals that the sample data from the statistical model represents the original data. We prove this by using data for particular times we are sure of the nature of the duct. These times are midnight when the ground, a good conductor, will have loosed heat and the speed of sound on the ground is lower than that above the ground, and in the evening when the ground is still hot due to the heat of the day. The midnight will have a good ground duct while the evening will have a bad ground duct. In the periods where we had a good ground duct, the KDEs peaked at about -70dB to -80dB, and a high probability is around this interval.

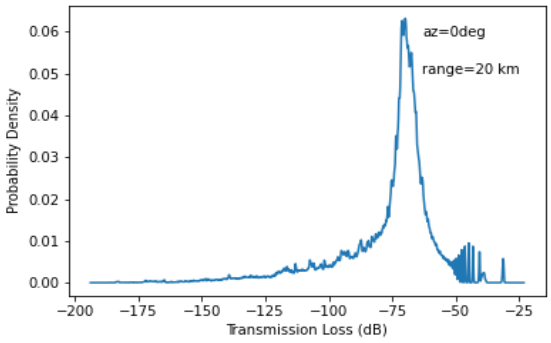

(i)

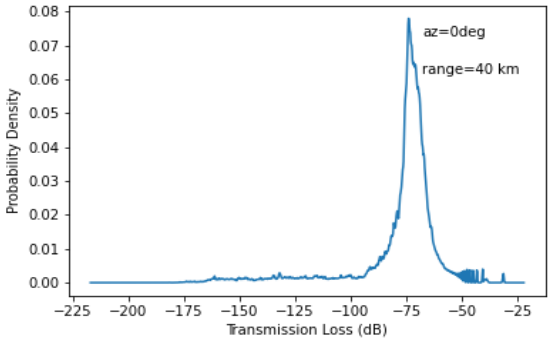

(ii)

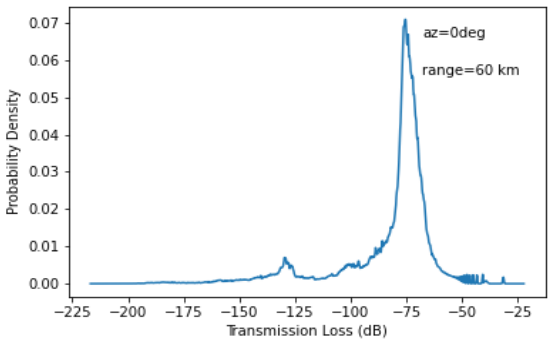

(iii)

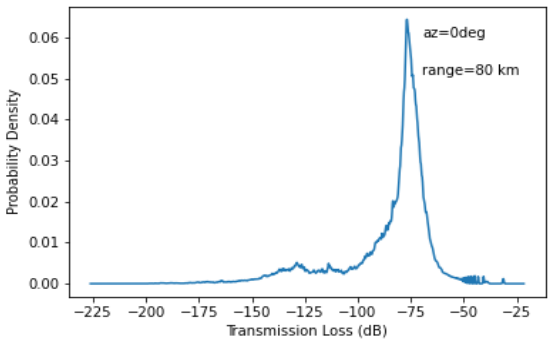

(iv)

Figure 5.1: Probability distribution for January 5th hour (UTC). This is for all days in the second week in the 0º propagation angle for maximum ranges of (i) 20 km, (ii) 40 km, (iii) 60 km, and (iv) 80 km.

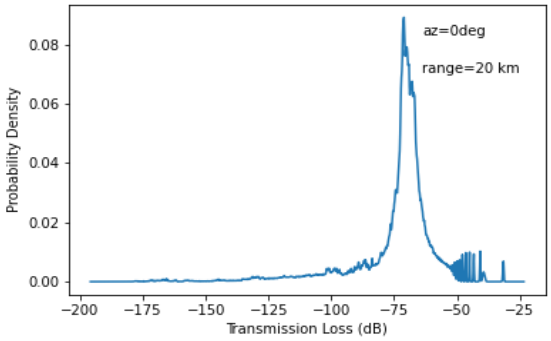

(i)

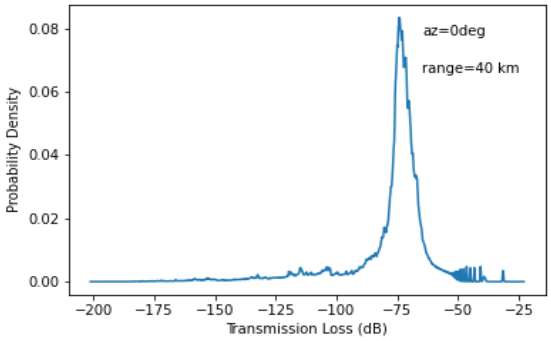

(ii)

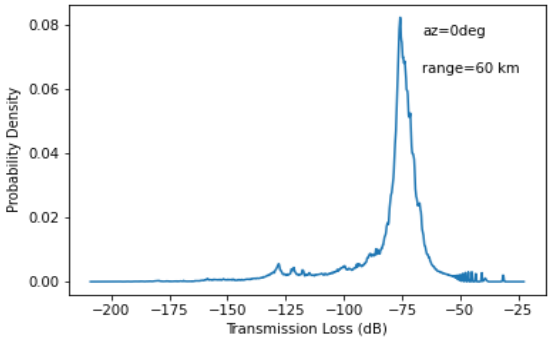

(iii)

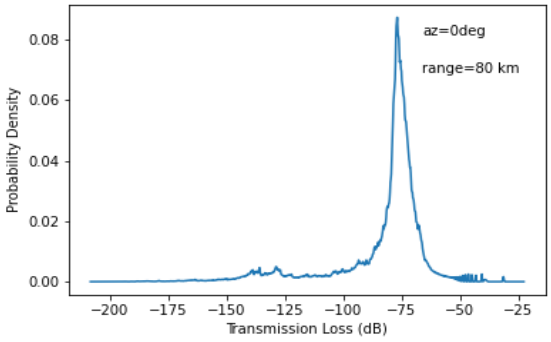

(iv)

Figure 5.2: Probability distribution for April 5th hour (UTC). This is for all days in the second week in the 0° propagation angle for maximum ranges of (i) 20 km, (ii) 40 km, (iii) 60 km and (iv) 80 km

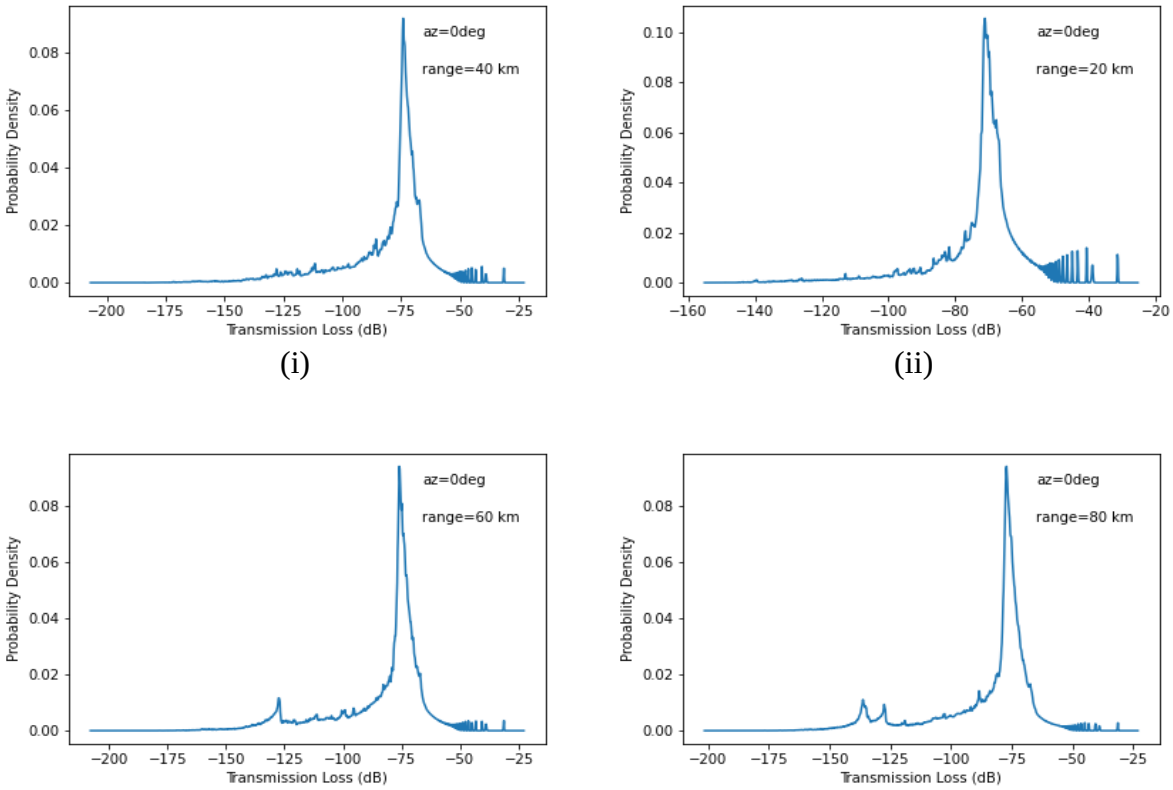

Figure 5.3: Probability distribution for August 5th hour (UTC). This is for all days in the second week in the 0° propagation angle for maximum ranges of (i) 20 km, (ii) 40 km, (iii) 60 km and (iv) 80 km.

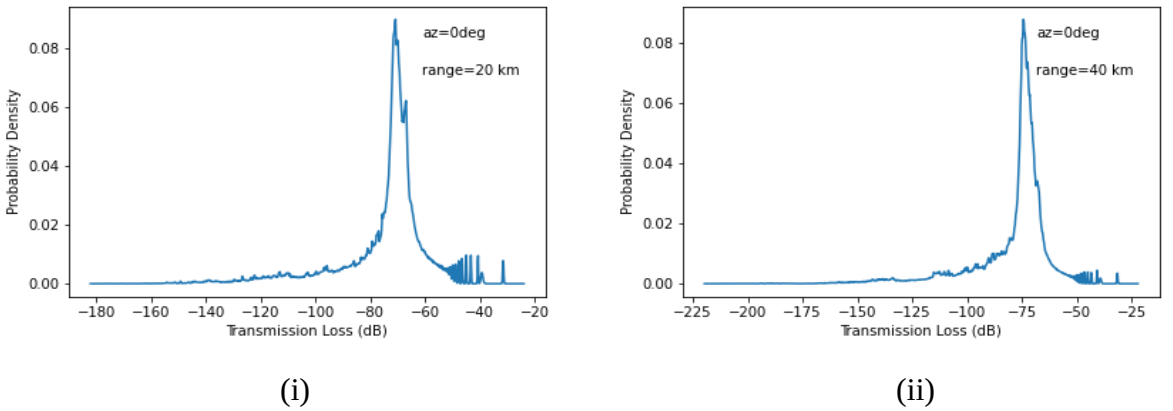

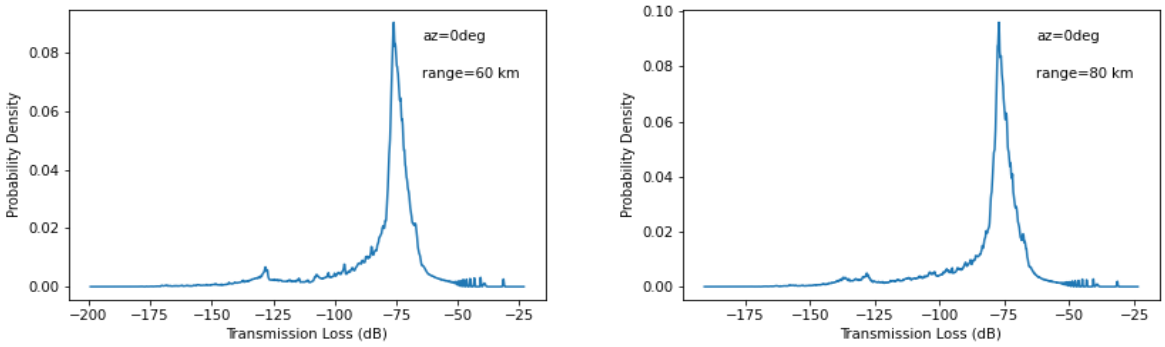

(iii) (iv)

Figure 5.4: Probability distribution for October 5th hour (UTC). This is for all days in the second week in the 0° propagation angle for maximum ranges of (i) 20 km, (ii) 40 km, (iii) 60 km and (iv) 80 km.

This was consistent for all months, even during the summer, when the tropospheric jet is less strong than in other seasons. The distance from the source of propagation doesn't really affect the days in which the ground ducts are good. But have effects on periods when ground ducts were very bad. This is obvious from the probability distributions.

Periods with a very bad ground duct showed a high probability for high transmission loss values compared to periods with a good ground duct. The probability of getting low transmission loss on these days when the ground duct was very bad, at greater distances than 20 km, is because of how the propagation model produces the transfer functions. It does this by

considering all the kilometers till we get to the range. That is for a range of 40 km; it outputs transfer functions for 1 km, 2 km, 3 km, and so on till 40 km. The following figures show these:

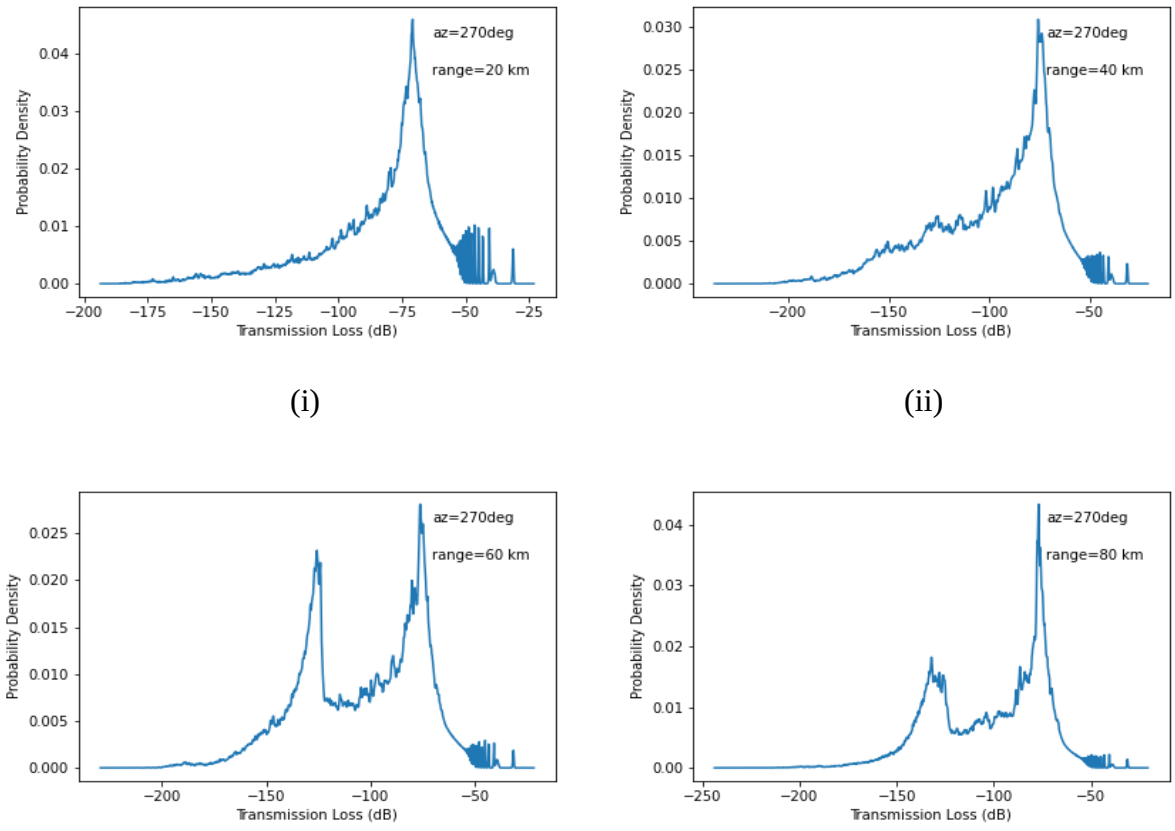

(i) (ii)

(iii) (iv)

Figure 5.5: Probability distribution for January, 23rd hour (UTC). This is for all days in the second week in the 270° propagation angle for maximum ranges of (i) 20 km, (ii) 40 km, (iii) 60 km and (iv) 80 km.

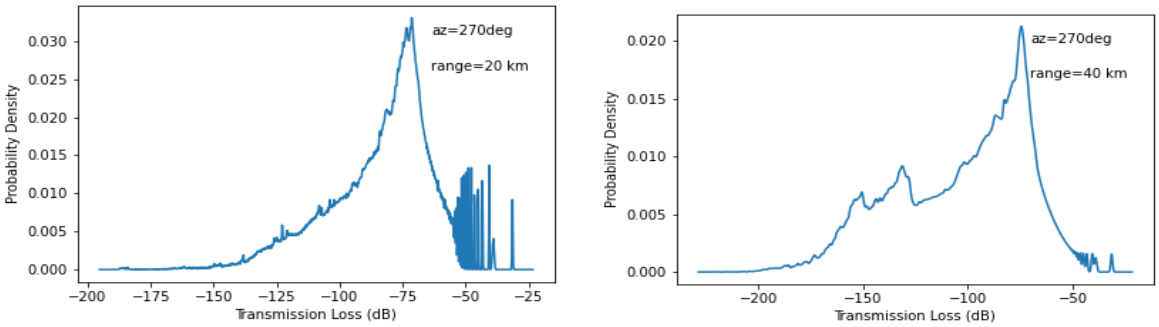

(i) (ii)

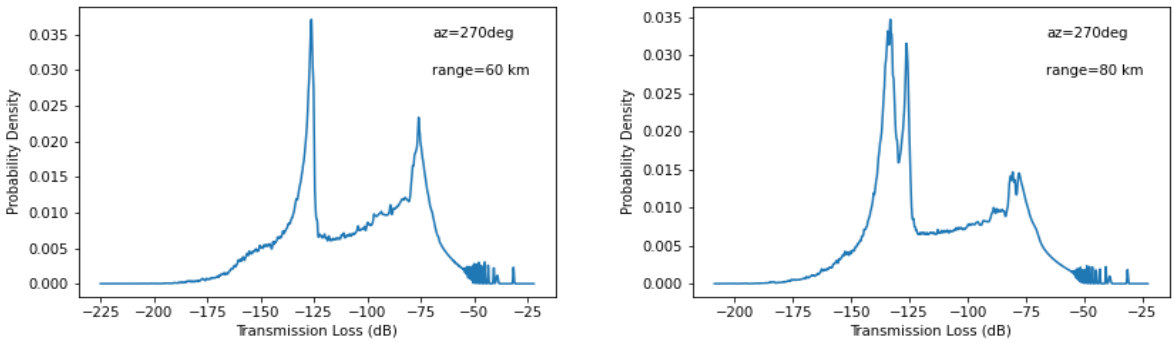

(iii) (iv)

Figure 5.6: Probability distribution for April, 23rd hour (UTC). This is for all days in the second week in the 270° propagation angle for maximum ranges of (i) 20 km, (ii) 40 km, (iii) 60 km and (iv) 80 km.

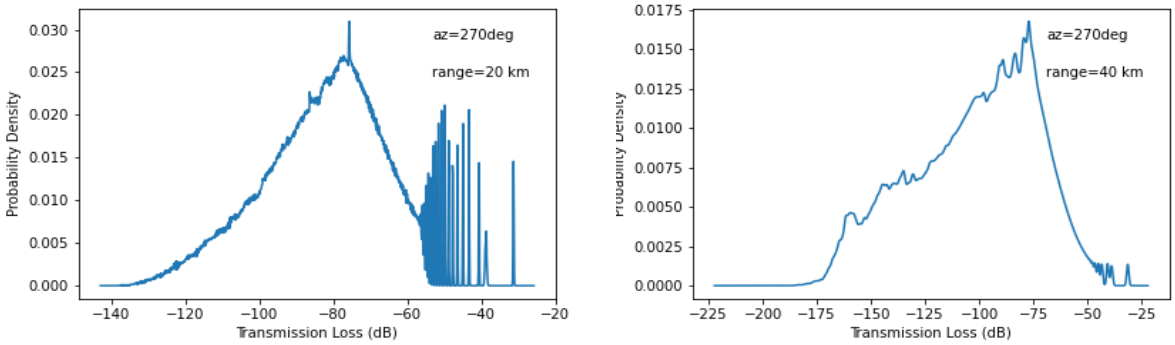

(i) (ii)

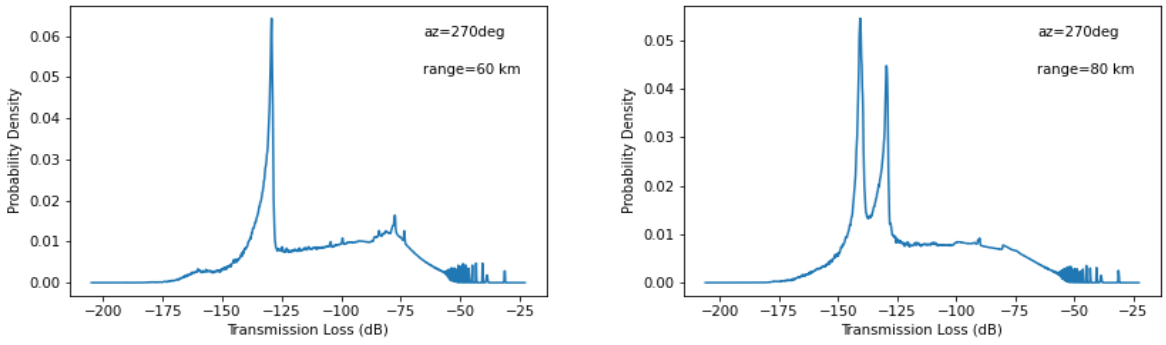

(iii) (iv)

Figure 5.7: Probability distribution for August, 23rd hour (UTC). This is for all days in the second week in the 270° propagation angle for maximum ranges of (i) 20 km, (ii) 40 km, (iii) 60 km and (iv) 80 km.

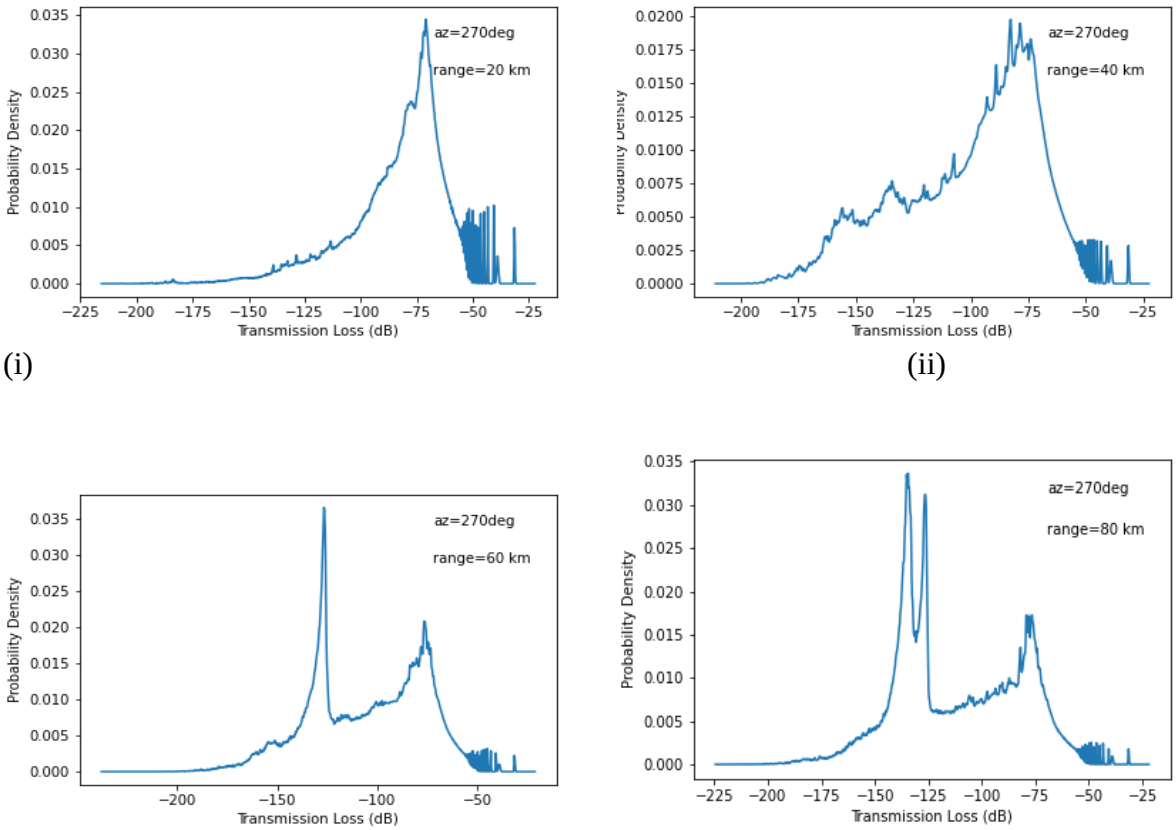

(i) (ii)

(iii) (iv)

Figure 5.8: Probability distribution for October, 23rd hour (UTC). This is for all days in the second week in the 270° propagation angle for maximum ranges of (i) 20 km, (ii) 40 km, (iii) 60 km and (iv) 80 km.

CHAPTER 6

FORMALISM FOR SIGNAL DETECTION

This session presents a formalism for signal detection using the signal-to-noise ratio. The signal-to-noise ratio is expressed in decibels. An example noise model developed by Maxwell Willis is seen in Figure 6.1. All months considered in the result chapter is considered here except August, replaced by July.

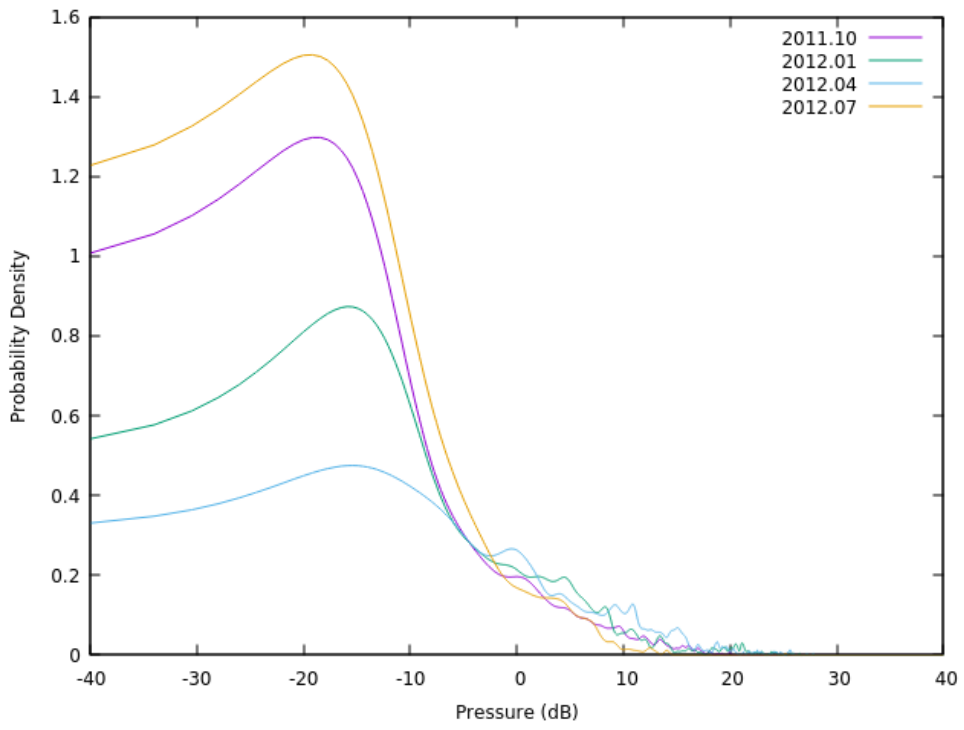

Figure 6. 1: Probability distribution for noise pressure for a sensor. This is in the frequency band of 0.4-4Hz for January, April, July, and October.

The signal-to-noise ratio (SNR) in decibels (dB) is given as

$$\mathrm{SNR_{dB}} = \mathrm{S_{dB}} + \mathrm{TL_{dB}} - \mathrm{N_{dB}} \tag{6.1}$$

the threshold for SNR is usually taken to be one; that is for us to have detection we should have

$$\mathrm{SNR} \geq 1 \tag{6.2}$$

but in dB, we will have

$$\mathrm{SNR_{dB}} \geq 0 \tag{6.3}$$

Hence the detection criterion is given as

$$\mathrm{S_{dB}} + \mathrm{TL_{dB}} - \mathrm{N_{dB}} \geq 0 \tag{6.4}$$

Furthermore, we can have

$$\mathrm{S_{dB}} \geq \mathrm{N_{dB}} - \mathrm{TL_{dB}} \tag{6.5}$$

Let

$$\mathrm{N_{dB}} - \mathrm{TL_{dB}} = \mathrm{Q} \tag{6.6}$$

Hence,

$$\mathrm{S_{dB}} \geq \mathrm{Q} \tag{6.7}$$

This is a criterion for detection that states that the source pressure has to be greater than or equal to the difference between noise level at the sensor and the transmission loss given as Q. Since we are studying this probabilistically, we have to use the probability distributions we have developed to get a criterion. To get the criterion, we get the expectation value for Q and standard deviation.

The standard deviation gives us a measure for our confidence in the expectation value gotten. A small deviation means we can trust the expected value, plus or minus the deviation. A large deviation means we cannot. The expectation value for Q is given as

$$< \mathrm{Q} > = \int_{-\infty}^{\infty} \mathrm{Q}\, \mathrm{P}(\mathrm{TL}, \mathrm{N}) \mathrm{dTL}\, \mathrm{dN} \tag{6.8}$$

$\mathrm{P}(\mathrm{TL}, \mathrm{N})$ is the joint probability density function of the transmission loss and noise. Taking a reasonable guess that these are independent, as what is happening to the signal propagating is quite different from the noise at the sensor, although in nature they have a relationship; we will have that the joint probability density function give us the product of the individual probability density functions

$$\mathrm{P}(\mathrm{TL}, \mathrm{N}) = \gamma(\mathrm{TL})\beta(\mathrm{N}) \tag{6.9}$$

Hence $< \mathrm{Q} >$ gives us

$$\int_{-\infty}^{\infty} \mathrm{Q}\, \gamma(\mathrm{TL})\beta(\mathrm{N})\, \mathrm{dTL}\, \mathrm{dN} \tag{6.10}$$

Substituting the value of Q and ignoring the dB subscripts in $\mathrm{N_{dB}}$ and $\mathrm{TL_{dB}}$, as our probability distribution is in terms of dB, we have

$$< \mathrm{Q} > = \int_{-\infty}^{\infty} (\mathrm{N} - \mathrm{TL})\, \beta(\mathrm{N})\, \gamma(\mathrm{TL})\, \mathrm{dTL}\, \mathrm{dN} \tag{6.11}$$

Given that

$$\int_{-\infty}^{\infty} \beta(\mathrm{N})\, \mathrm{dN} = 1 \tag{6.12}$$

and

$$\int_{-\infty}^{\infty} \gamma(\mathrm{TL})\, \mathrm{dTL} = 1 \tag{6.13}$$

(6.11) will give us

$$< Q > = \int_{-\infty}^{\infty} N\ \beta(N)\ dN - \int_{-\infty}^{\infty} TL\ \gamma(TL)\ dTL \tag{6.14}$$

Thus, we have

$$< Q > = < N > - < TL > \tag{6.15}$$

This gives us that the expectation value for the difference between noise and transmission loss is the difference between the expectation value of noise and the expectation value of transmission loss.

To measure the confidence in this average, we find the standard deviation of the joint probability distribution. This is just the square root of the variance of the distribution.

The variance is given as

$$\int_{-\infty}^{\infty} (N - TL - < N > + < TL >)^2\ P(TL, N)\ dTL\ dN \tag{6.16}$$

After some simplification, we have

$$< (N - < N >)^2 > + < (TL - < TL >)^2 > \tag{6.17}$$

This gives us that the variance of the joint distribution is the sum of the variance of noise and variance of transmission loss.

Standard deviation will hence give us

$$(< (N - < N >)^2 > + < (TL - < TL >)^2 >)^{\frac{1}{2}} \tag{6.18}$$

The standard deviation in (6.18), as discussed earlier, gives us a measure of confidence in the expectation value of Q, the detection criterion. A small deviation tells us we can trust the expected value, plus or minus the deviation. A large deviation means we cannot trust the expectation value.

CHAPTER 7

CONCLUSION

This thesis presents a way to sample using EOF analysis and inverse transform. This works for cases where we have coefficients of the EOFs which are statistically independent, and we can see that this works from the probability distributions displayed in the result session. The periods with good duct showed a high probability for low transmission loss values and vice versa.

Also, from the previous chapter, we can see that we can develop a detection criterion using the signal-to-noise ratio. Further, we find a formalism to get an expectation value to use in the detection criterion, given we have the noise model. Also, we find a way to measure our confidence in the expectation value.

In real-life applications, this project can be used to predict if a sensor at a region at some particular time will detect signal given that we have a noise model for the sensor and we know what the source pressure is. Also, it is useful in knowing what the pressure level of the source should be so we can detect signals at a sensor placed at a particular location.

LIST OF REFERENCES

LIST OF REFERENCES

[1] M. Willis. *Tropospheric Ducting and its Effect on Infrasonic Propagation*. MS thesis, University of Mississippi, 2018.

[2] R. Waxler. An overview of infrasound propagation. *Internoise, Hamburg*, 2016.

[3] J. D. Assink, R. Waxler, D. Velea. A wide-angle high Mach number modal expansion for infrasound propagation. *The Journal of the Acoustical Society of America*, 141(3):1781-1792, 2017.

[4] A. Le Pichon, E. Blanc, A. Hauchecorne, editors. *Infrasound Monitoring for Atmospheric Studies: Challenges in Middle Atmosphere Dynamics and Societal Benefits*. Springer, International Publishing AG, 2019.

[5] W. C. Skamarock, J. B. Klemp, J. Dudhia, D. O. Gill, Z. Liu, J. Berner, W. Wang, J. G. Powers, M. G. Duda, D. M. Barker, and X.-Y. Huang. A Description of the Advanced Research WRF Version 4. NCAR Tech. Note NCAR/TN-556+STR, 145 pp, 2019.

[6] R. Waxler, C. Hetzer, J. D. Assink, D. Velea. chetzer-ncpa/ncpaprop-release: NCPAprop v2.1.0 (v2.1.0). *Zenodo*, 2021.

[7] S. L. Brunton and J. N. Kutz. *Data-Driven Science and Engineering: Machine Learning, Dynamical Systems, and Control*. Cambridge University Press, 2019.

[8] D. Donoho and M. Gavish. The Optimal Hard Threshold for Singular values is. *IEEE Transactions on Information Theory*, 60. 10.1109/TIT.2014.2323359, 2013.

[9] A. Dawson. eofs: A Library for EOF Analysis of Meteorological, Oceanographic, and Climate Data. *Journal of Open Research Software*, 4(1), p.e14, 2016.

VITA

Adedotun Lawal

Education

2018 - B.S. in physics at the University of Lagos

Academic Employment

2020 - 2021 – Teaching Assistant in General Physics courses, Department of Physics and Astronomy, University of Mississippi: Introduced students to electricity and magnetism through laboratory curriculum and graded homework and exams.

2021 - 2022 – Research Assistant, Infrasound Group at the National Center for Physical Acoustics: Worked under Roger Waxler, PhD, to develop statistical models for signal detection.